PHYSICAL REVIEW D VOLUME 23, NUMBER 9 1 MAY 1981

Coherent proton diffraction dissociation on helium from 46 to 400 GeV

A. Bujak,* P. Devensky,† A. Kuznetsov, B. Morozov, V. A. Nikitin, P. Nomokonov, Y. Pilipenko, and V. Smirnov
Joint Institute for Nuclear Research, Dubna, U.S.S.R.

E. Jenkins
University of Arizona, Tucson, Arizona 85721

E. Malamud, M. Miyajima,‡ and R. Yamada
Fermi National Accelerator Laboratory, Batavia, Illinois 60510

A. Sandacz
Institute of Nuclear Research, Warsaw, Poland
(Received 17 June 1980)

Inclusive coherent proton diffraction dissociation on helium has been measured in the four-momentum transfer and missing-mass region $0.04 < |t| < 0.40$ (GeV/c)^2, $M_X{}^2 < 10$ GeV^2 and for incident proton beam momenta from 46 to 400 GeV/c. We find that the differential cross section $d^2\sigma/dt\,dM_X{}^2$ varies slowly with energy, reveals a pronounced peak at $M_X{}^2 \simeq 2$ GeV^2, and at large masses behaves approximately as $1/M_X{}^2$. The cross section falls exponentially as $|t|$ increases, with a large slope parameter at small momentum transfers and a substantially smaller one at large $|t|$ values, with no clear dip between the two regions as seen in elastic scattering. We compare the experimental t distributions to Glauber-model predictions and find the data provide a sensitive test of the assumptions on the details of the elementary proton diffraction-dissociation amplitudes and on the total cross sections of the diffractively produced states.

I. INTRODUCTION

In an experiment performed at the Fermi National Accelerator Laboratory we have measured the inclusive reaction

$$p\,{}^4\mathrm{He} \to X\,{}^4\mathrm{He} \tag{1}$$

at incident proton momenta $46 < p_{\mathrm{beam}} < 400$ GeV/c, and at momentum transfers and missing masses covering the ranges $0.04 < |t| < 0.40$ (GeV/c)^2 and $(m_p + m_\pi)^2 < M_X{}^2 < 10$ GeV^2.

Recently, at the same energies and in a similar momentum-transfer interval new precise data on elastic proton-helium scattering were published.[1] A comparison of both diffractive processes, especially in the t range where multiple-scattering effects are important, may illuminate the similarities and differences between both processes. The main features of elastic proton-helium scattering, i.e., a sharp decrease of the cross section at small $|t|$ values, and the presence of a dip and secondary maximum, can be reproduced[1] using Glauber analysis with a nucleon-nucleon elastic-scattering amplitude that is predominantly imaginary, spinless, and central (in impact-parameter space).

As for coherent diffraction dissociation on nuclei, it was first observed for nucleon diffraction dissociation on deuterons at the CERN ISR[2] that the data disagree with Glauber-model predictions with central elementary nucleon diffraction dissociation but agreement can be obtained if peripheral (in impact-parameter space) and spin-dependent elementary diffraction-dissociation amplitudes are used.

One of our objectives in studying reaction (1) is to see if these conclusions hold for coherent diffraction dissociation on helium. Another interesting possibility which can be investigated with helium data is the propagation of diffractively produced states in nuclear matter and the related problem of the total cross section for diffractive states on nucleons. Due to the compactness of the helium nucleus and the large contribution of multiple-scattering effects, one can expect helium data to be sensitive to how the diffractively produced states interact before leaving the nucleus.

Earlier results on two similar reactions at Fermilab energies have been reported, namely inclusive proton dissociation on protons,[3-7]

$$pp \to Xp\,, \tag{2}$$

and on deuterons,[7,8]

$$pd \to Xd\,. \tag{3}$$

Combined analysis of proton diffraction dissociation on different targets in reactions (1)–(3) may yield information on exchanges of different quantum numbers in proton excitation.

In Sec. II we describe the experiment and details of data analysis. In Sec. III we present our experimental results and discuss some results of phenomenological fits to the data. The Glauber analysis using both central and peripheral amplitudes

of elementary diffraction dissociation is described in Sec. IV. In Sec. V we summarize our conclusions.

II. EXPERIMENTAL PROCEDURE AND DETAILS OF DATA ANALYSIS

The data were taken in an experiment with the circulating internal proton beam intercepting a helium gas jet. Recoil particles were detected by sets of sandwiches of silicon semiconductor detectors.

The experiment was primarily designed and performed to study p ^{4}He elastic scattering[1] but coherent diffraction dissociation of incident protons on helium was measured simultaneously. The detailed description of the experimental setup and apparatus is published elsewhere.[1] In the present paper we discuss details relevant for inelastic data analysis.

The gas-jet target was viewed at angles $\omega = 0$–120 mrad from a direction perpendicular to the beam, by sets of totally depleted surface-barrier silicon detectors. The front detectors ranged in thickness from 15 to 200 μm and the back detectors from 200 to 2000 μm. The detectors were placed on a movable carriage at a distance 7.2 m from the target yielding angular acceptance $\Delta\omega = 0.7$ mrad. The uncertainty in angle was less than about ± 0.2 mrad. The detectors were calibrated with a $^{234}_{90}$Th α-particle source and also by using elastic peaks and the geometry of the experiment. The uncertainty of energy calibration is less than $\pm 1.5\%$. The detector energy resolution was 50–150 keV.

To identify recoil particles, for each detector sandwich we sorted recoils into plots of the front detector energy T_F vs back detector energy T_B. Only recoils stopping in the rear detector were analyzed. For each event we determined a recoil-mass identification parameter I,

$$I = T_F g(T_B) + h(T_B) , \tag{4}$$

where g and h are polynomial functions of T_B, determined in such a way that for the centers of gravity of the ^{4}He band on the scatter plot $I = 4$ and for ^{3}He $I = 3$. In Fig. 1 a typical I parameter plot on a logarithmic scale is shown for a detector sandwich. ^{4}He recoils were defined by the cut $3.5 < I < 4.5$. The separation between ^{4}He and ^{3}He recoils is excellent over all t intervals studied. The contamination from ^{3}He is less than 1% for the thinnest sandwiches and is negligible (< 0.5%) for the thick ones.

Two permanently fixed stacks detecting elastic events were used to monitor the jet-beam interaction rate. The normalization of differential cross sections for reaction (1) was found using simultaneously measured proton-helium elastic events and published cross sections.[1] The normalization errors of our inelastic cross sections are ±4 to 5 % for each incident energy.

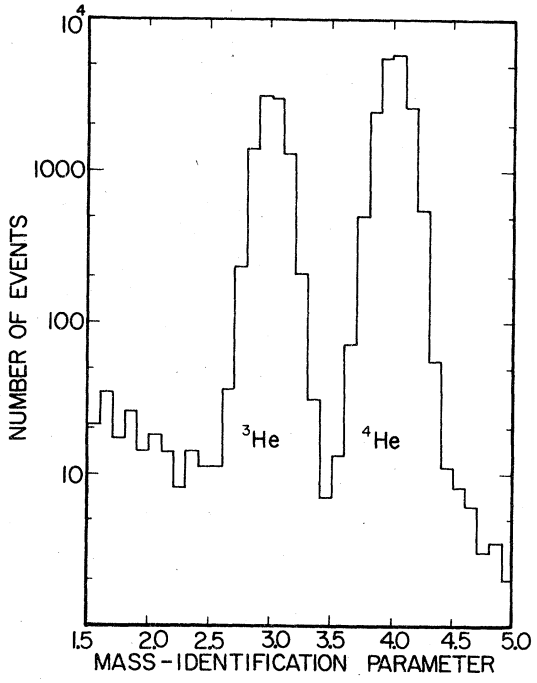

FIG. 1. Mass-identification-parameter I distribution for a detector sandwich consisting of a 190-μm front detector and a 1500-μm back detector (data combined from several different angular positions).

The main source of background for reaction (1) is the elastic scattering from residual helium gas outside the target region. The residual gas density varies slowly with angle and is typically less than 10% of the density in the gas jet. We eliminated this background by applying a momentum-transfer- and beam-momentum-dependent cut on missing mass $M_X^2 > M_{X\,\mathrm{min}}^2$, where

$$M_{X\,\mathrm{min}}^2 \simeq m_p^2 + 2p_{\mathrm{beam}} \sqrt{|t|}\,\omega_a . \tag{5}$$

The parameter ω_a is the angular size of the downstream part of the aperture, i.e., from the jet target to the most downstream point in the accelerator main ring as seen by the detector. It is equal to 11 mrad and it does not depend significantly on the detector and its angular position. The maximum missing mass we can measure is determined by the maximum accessible angle ω, and linearly increases with beam momentum. The mass ranges overlap for close beam momenta and move to higher masses as momentum increases. For example, at $t = -0.1$ (GeV/c)^2 and the lowest beam momentum 46 GeV/c, the missing-mass

TABLE I. Missing-Mass Resolution $\Delta(M_X^2)$ in GeV^2 as a function of p_{beam}, M_X^2, and t.

M_X^2 (GeV^2) \ p_{beam} (GeV/c)	46		97		259		347	
$-t$ (GeV/c)^2	0.05	0.40	0.05	0.40	0.05	0.40	0.05	0.40
1.2	0.07	0.08	0.04	0.09				
1.4	0.17	0.18	0.09	0.12				
3.0			0.14	0.16	0.10	0.24		
5.0					0.13	0.25	0.13	0.32
9.0					0.21	0.30	0.18	0.34

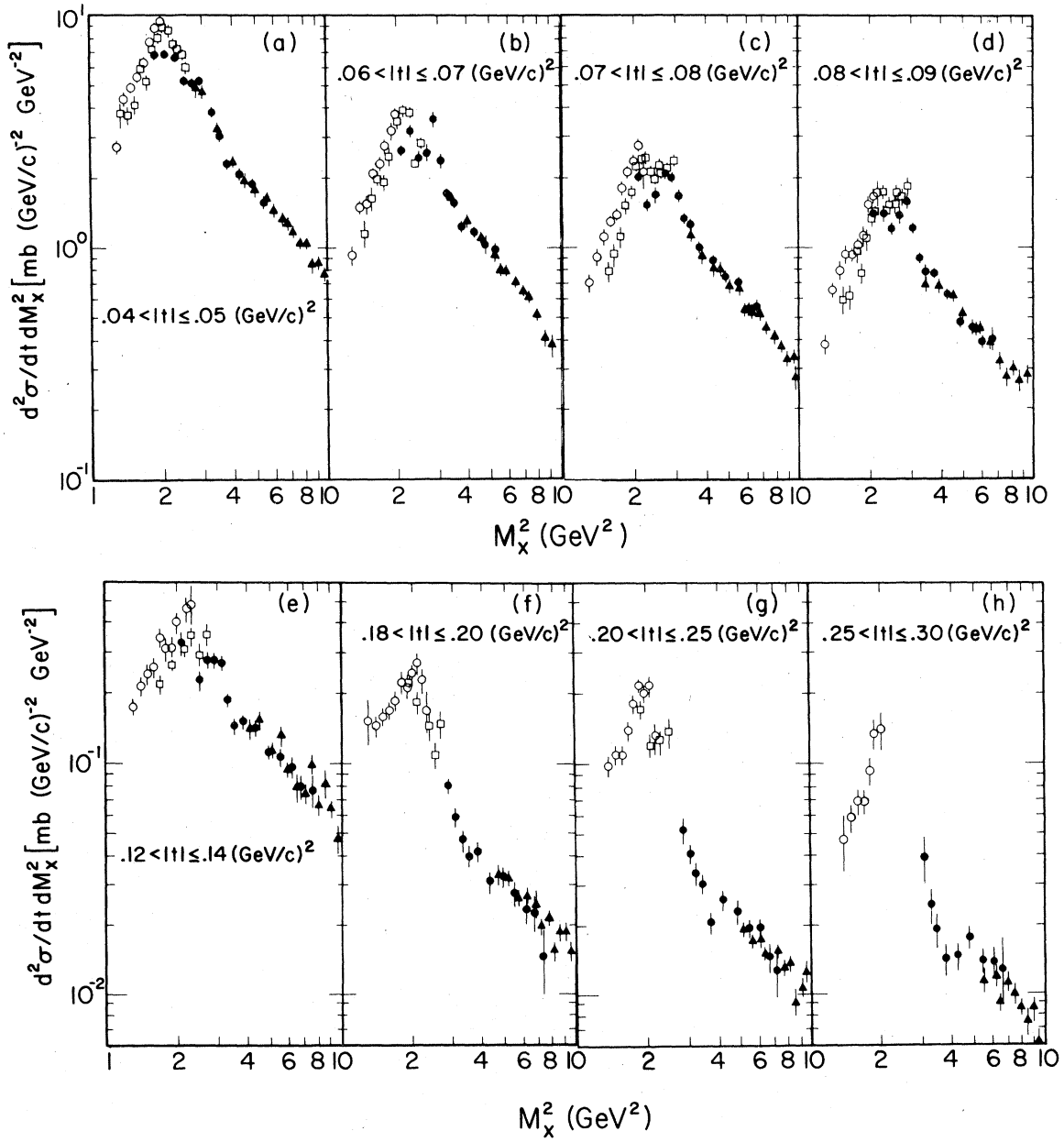

FIG. 2. Differential cross sections as functions of M_X^2 in different t intervals. Different symbols correspond to cross sections at four incident momenta: ○, 46 GeV/c; □, 97 GeV/c; ●, 200 GeV/c; ▲, 394 GeV/c.

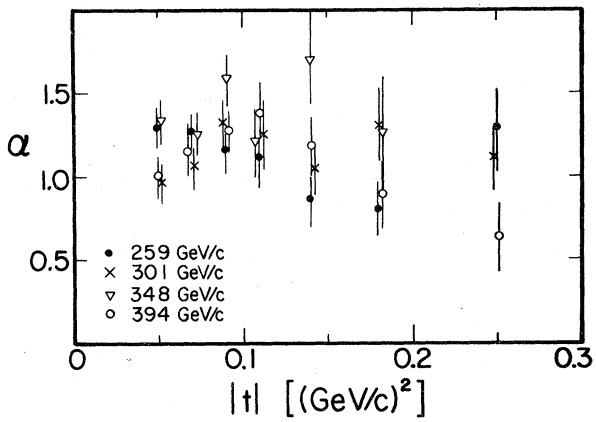

FIG. 3. Fitted values of the parameter α as obtained from the fit $d^2\sigma/dt\,dM_X^2 \mid_{t\,\text{fixed}} = A/(M_X^2)^\alpha$ to the large-mass data $5.0 < M_X^2 \leq 7.5$ GeV^2.

range is $1.2 < M_X^2 < 2.2$ GeV^2 and for the highest momentum 394 GeV/c, it is $3.7 < M_X^2 < 13.0$ GeV^2.

Another important source of background is inelastic events from residual gas. To evaluate this background we folded the density of residual gas (determined from the data at 46 GeV/c, where the separation between elastic and inelastic events is sufficiently good) with measured diffraction-dissociation cross sections at different t, M_X^2 and beam-momentum values. It turned out that at small masses ($M_X^2 < 5$ GeV^2) this background has complicated t, mass, and momentum dependence and it oscillates around the average value 9% of the inelastic contribution from the target. For large masses the background is nearly constant and equal to about 9%. The data were corrected for this average inelastic background. For large masses this correction practically removes the inelastic background; for small masses it substantially reduces its contribution to less than ±6%.

The experimental momentum-transfer resolution is less than ± 0.001 (GeV/c)^2. Due to errors in detector calibration the maximum systematic error on t is $(\Delta t/t) \pm 1.5\%$.

The missing-mass resolution is mainly determined by the detector angular acceptance $\Delta\omega = 0.7$ mrad and the binning of incident momentum $\Delta p_{\text{beam}} \leq 16$ GeV/c. In our acceptance region the missing-mass resolution ΔM_X^2 varies between ± 0.05 and ± 0.34 GeV^2, depending on M_X^2, t and p_{beam}; in general, it increases with increasing t or M_X^2. Table I illustrates the missing-mass-resolution dependence on M_X^2, t, and p_{beam}. The systematic errors on M_X^2 are due to systematic errors on angle and recoil energy. In our t range they increase from ± 0.005 to ± 0.07 GeV^2 for small missing masses and low incident momenta, and from ± 0.015 to ± 0.2 GeV^2 for large masses and high momenta.

III. EXPERIMENTAL RESULTS

A. Missing-mass distributions

We obtained differential cross sections for coherent proton diffraction dissociation on helium for the following incident momenta: 46, 97, 200, 259, 301, 348, and 394 GeV/c.

The differential cross sections, as functions of missing mass at different t intervals, are displayed in Figs. 2(a)–2(h). As discussed in Sec. II, at different momenta our data cover different mass ranges, so to show the mass dependence in a wide interval we plotted together the cross sections for four incident momenta: 46, 97, 200, and 394 GeV/c.

The pronounced peak at $M_X^2 \simeq 2$ GeV^2 dominates cross sections at almost all t values. The bump at 2.8 GeV^2 can be seen at small momentum transfers and its relative contribution is largest at $|t| = 0.07$–0.09 (GeV/c)^2 where it becomes comparable to the peak at 2 GeV^2. At large masses ($M_X^2 > 4$ GeV^2), the cross sections drop approximately as $1/M_X^2$. A peculiar feature of the data is the behavior of the ratio between cross sections for the peak at 2 GeV^2 and for the high-mass tail. At small momentum transfers this ratio decreases with increasing $|t|$ for $|t| < 0.14$ GeV/c^2, but at high momentum transfers it becomes even larger than for the smallest $|t|$ values.

For large masses the following formula was fitted to the cross sections:

$$\left.\frac{d^2\sigma}{dt\,dM_X^2}\right|_{t\,\text{fixed}} = \frac{A}{(M_X^2)^\alpha}, \tag{6}$$

where A and α are fitted parameters. The fitted values of α for different momenta and t values are plotted in Fig. 3. All mass distributions were fitted in the same range, $5 < M_X^2 < 7.5$ GeV^2, for all t intervals and momenta. Within errors the parameter α does not depend on energy and t. The mean value for all energies and t intervals is $\alpha_{\text{mean}} = 1.18 \pm 0.03$. If we included (where it was possible) in our fits the data at the highest masses ($M_X^2 > 7.5$ GeV^2) the parameter became slightly lower. In the framework of the triple-Regge model the $1/M_X^2$ behavior of the cross section reflects the dominance of triple-Pomeron coupling in process (1). The fact that $\alpha \neq 1$, as well as some energy dependence of the cross sections, suggests that non-triple-Pomeron couplings cannot be neglected.

B. Four-momentum-transfer distributions

The t distributions for different missing-mass ranges are shown in Figs. 4(a)–4(h). The cross

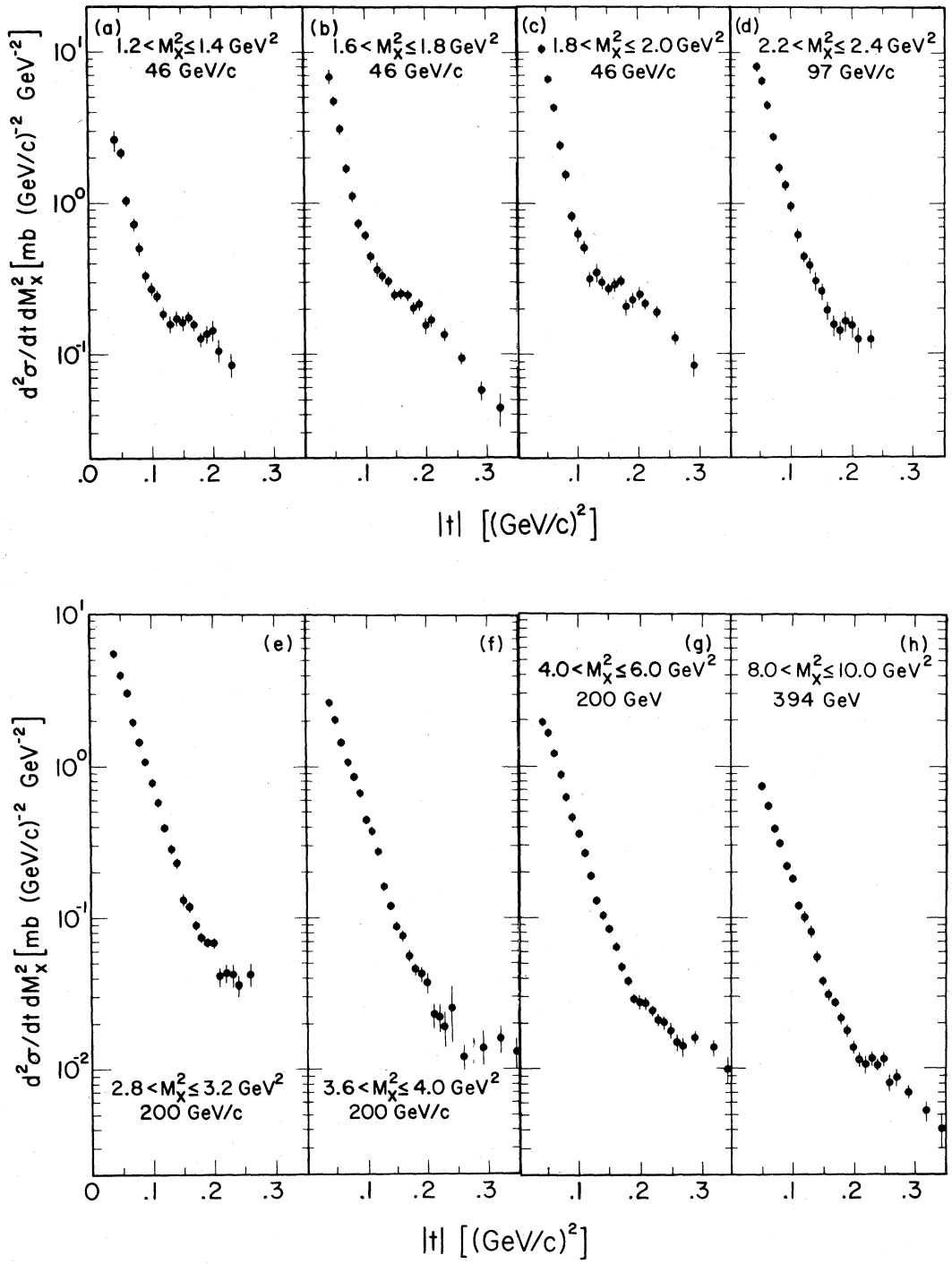

FIG. 4. Differential cross sections as functions of t in different M_X^2 intervals.

sections drop 2–3 orders of magnitude in the measured t range with no clear evidence of a dip as seen in elastic scattering.[1] A kink appears at $|t| \approx 0.1$–0.2 $(\mathrm{GeV}/c)^2$. The cross section can be described as a sum of two exponentials. At small t values it decreases with a slope parameter equal to 30–60 $(\mathrm{GeV}/c)^{-2}$ and at high momentum transfers with slope 5–10 $(\mathrm{GeV}/c)^{-2}$.

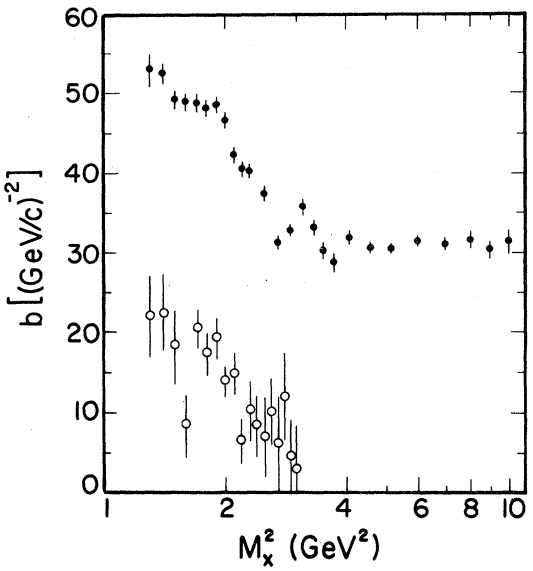

FIG. 5. Fitted values of the slope parameter. Black points obtained from the fit $(d^2\sigma/dt\,dM_X^2)\,|\,M_X^2{}_{\text{fixed}} = Ae^{b(t+0.065)}$ in the t range $0.04 < |t| \leq 0.08$ (GeV/c)^2 for the reaction $p\,^4\text{He} \to X\,^4\text{He}$. Open points are the slope parameter for the reaction $p\,p \to Xp$ (Ref. 4).

The details of this pattern show an interesting mass dependence. To study this dependence the data were fitted with the formula

$$\left.\frac{d^2}{dt\,dM_X^2}\right|_{M_X^2\text{fixed}} = A_1 \exp[B_1(t+0.1)] + A_2 \exp[B_2(t+0.3)]. \quad (7)$$

The fitted B_1 and B_2 parameters do not depend on energy within error limits. B_1 decreases monotonically as the mass increases, from 60 (GeV/c)$^{-2}$ at $M_X^2 \simeq 1.5$ GeV^2 to 33 (GeV/c)$^{-2}$ at $M_X^2 \simeq 4$ GeV^2 and stays constant for higher masses. The B_2 parameter varies similarly. It decreases from 10 (GeV/c)$^{-2}$ at $M_X^2 \simeq 1.5$ GeV^2 to 5 (GeV/c)$^{-2}$ at $M_X^2 \simeq 3$ GeV^2 and becomes approximately constant at higher masses. The kink shifts from $|t| \simeq 0.1$ (GeV/c)^2 at the smallest masses to $|t| \simeq 0.2$ (GeV/c)^2 at $M_X^2 \geq 4$ GeV^2.

To compare our results for the slope parameter with existing data on the $pp \to Xp$ (Ref. 4) and $pd \to Xd$ (Ref. 8) reactions, a one-exponential fit was done for the low-t cross sections,

$$\left.\frac{d^2\sigma}{dt\,dM_X^2}\right|_{M_X^2\text{fixed}} = A \exp[b(t+0.065)] \quad (8)$$

in the t range $0.04 < |t| \leq 0.08$ (GeV/c)^2. Within our total errors the b parameter does not depend on energy. In Fig. 5 and in Table II we present the b dependence on M_X^2 with b parameters averaged over incident momenta. The errors are statistical. The systematic errors on b at small masses are less than ± 1.5 (GeV/c)$^{-2}$ and at large masses ($M_X^2 > 5$ GeV^2) they are negligible. The slope parameter is equal to ≈ 50 (GeV/c)$^{-2}$ at the smallest masses, about 45 (GeV/c)$^{-2}$ at $M_X^2 \approx 2$ GeV^2, and then quickly drops as the mass increases and flattens out at $b \approx 31$ (GeV/c)$^{-2}$ for $M_X^2 \geq 4$ GeV^2.

TABLE II. Slope parameter[a] as a function of mass, $0.04 < |t| < 0.08$ (GeV/c)^2.

M_X^2 (GeV^2)	b [(GeV/c)$^{-2}$]	M_X^2 (GeV^2)	b [(GeV/c)$^{-2}$]
1.3	53.2 ± 2.1	2.9	32.9 ± 0.7
1.4	52.5 ± 1.2	3.1	35.9 ± 1.2
1.5	49.4 ± 1.0	3.3	33.4 ± 0.9
1.6	49.0 ± 1.0	3.5	30.4 ± 0.9
1.7	48.9 ± 0.9	3.7	28.8 ± 1.2
1.8	48.2 ± 1.0	4.1	31.7 ± 0.6
1.9	48.6 ± 1.0	4.6	30.4 ± 0.6
2.0	46.7 ± 0.8	5.2	30.5 ± 0.5
2.1	42.4 ± 0.8	6.0	31.5 ± 0.5
2.2	40.5 ± 0.7	7.0	31.1 ± 0.6
2.3	40.3 ± 0.9	8.0	31.7 ± 1.0
2.5	37.5 ± 0.8	9.0	30.3 ± 1.3
2.7	31.1 ± 0.8	10.0	31.5 ± 1.5

[a]See Eq. (8) in text.

We compared the slope-mass correlation for our data to those of Ref. 4 for reaction (2). The open points in Fig. 5 are slope parameters from proton target data. We observe a similar slope-mass correlation for proton and helium data.

C. Energy dependence

Due to the limited number of energies available for each missing mass and to systematic errors, it was not feasible to determine precisely the energy dependence of the data for each t and M_X^2 interval independently. But within the limits of errors one can conclude that the shapes of the t and mass distributions do not depend on energy, and the energy dependence of the cross sections is consistent with the formula

$$\frac{d^2\sigma}{dt\,dM_X^2} = \left(1 + \frac{28 \pm 4}{p_{\text{beam}}}\right) f(t, M_X^2). \quad (9)$$

The energy dependence is illustrated in Fig. 6. In Fig. 6(a) we have plotted $A = d^2\sigma/dt\,dM_X^2\,|_{t=-0.065(\text{GeV}/c)^2}$ determined from the fit of formula (8), as a function of M_X^2 and incident momentum. In Fig. 6(b) are shown corresponding cross sections reduced to the momentum 300 GeV/c according to the formula

$$A' = A\left(1 + \tfrac{28}{300}\right) \Big/ \left(1 + \frac{28}{p_{\text{beam}}}\right). \quad (10)$$

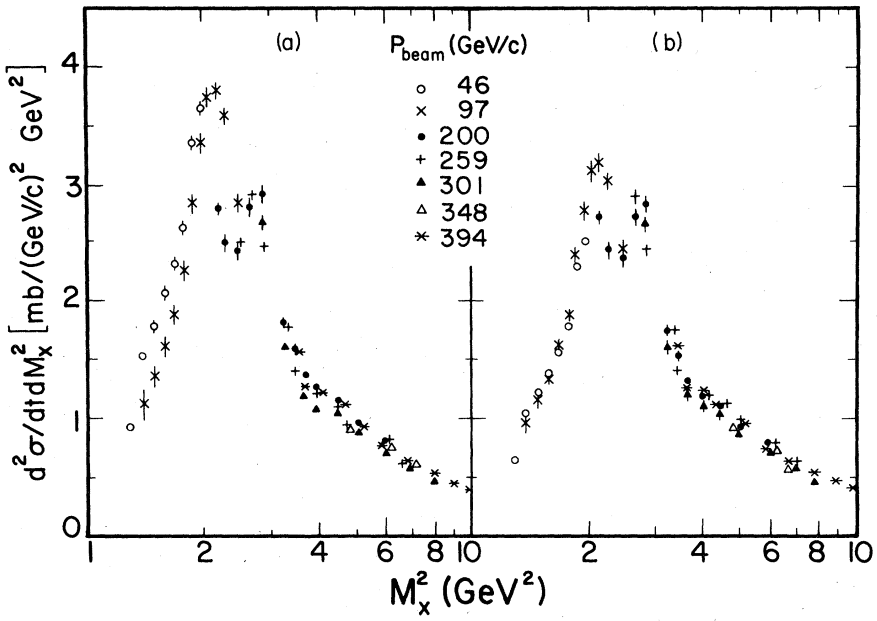

FIG. 6. (a) $A = (d^2\sigma/dt\,dM_X^2)|_{t=-0.065\ (\mathrm{GeV}/c)^2}$ as a function of M_X^2 and incident momentum. (b) The same as (a) except reduced to 300 GeV/c using $A' = A(1+\frac{28}{300})/[1+(28/p_{\mathrm{beam}})]$. All errors are statistical.

D. Cross sections

In Table III we present the cross sections at four incident momenta: 46, 97, 230, and 347 GeV/c. The data at 230 GeV/c are averaged over 200 and 259 GeV/c and the data at 347 GeV/c are averaged over 301, 348, and 394 GeV/c.

For each missing-mass range and incident momentum, we have listed the cross sections as a function of t. The listed errors are statistical. The normalization errors are about equal to ±5%. Small mass data ($M_X^2 < 5$ GeV^2) have additional systematic errors of less than ±6%, which are due to inelastic background from the residual gas.

The quoted errors refer to the relative normalization of inelastic cross sections. To account for the absolute normalization one has to include also systematic normalization errors of elastic proton-helium scattering[1] which are ±4.8%.

IV. GLAUBER ANALYSIS OF THE DIFFERENTIAL CROSS SECTIONS

A. Basic formulas

For coherent production $p\,{}^4\mathrm{He} \to X\,{}^4\mathrm{He}$, where X is a state with specified missing mass, we used the following Glauber formula[9-11] for the amplitude:

$$F(\vec{q}) = \frac{ip}{2\pi} e^{R^2q^2/16} \int d^2b\, e^{i\vec{q}\cdot\vec{b}} |\psi(\vec{r}_1,\vec{r}_2,\vec{r}_3,\vec{r}_4)|^2 \prod_{i=1}^{4} d^3r_i$$
$$\times\Big[\sum_i \Gamma_i^d - \sum_{i<j}(\Gamma_i^e\Gamma_j^d + \Gamma_j^d\Gamma_j^{e*}) + \sum_{i<j<k}(\Gamma_i^e\Gamma_j^e\Gamma_k^d + \Gamma_i^e\Gamma_j^d\Gamma_k^{e*} + \Gamma_i^d\Gamma_j^{e*}\Gamma_k^{e*})$$
$$-(\Gamma_1^e\Gamma_2^e\Gamma_3^e\Gamma_4^d + \Gamma_1^e\Gamma_2^e\Gamma_3^d\Gamma_4^{e*} + \Gamma_1^e\Gamma_2^d\Gamma_3^{e*}\Gamma_4^{e*} + \Gamma_1^d\Gamma_2^{e*}\Gamma_3^{e*}\Gamma_4^{e*})\Big], \tag{11}$$

where $\vec{q}$ is the momentum-transfer vector, p is the laboratory momentum of the projectile, $\vec{b}$ is the impact-parameter vector, $|\psi|^2$ is the helium density distribution, and $\vec{r}_l$ is the distance of the lth nucleon from the nucleus mass center. Γ_l is the profile function for the process $\alpha N \to \beta N$ on the lth target nucleon and the argument of Γ_l is $(\vec{b}-\vec{s}_l)$, where $\vec{s}_l$ is the transverse component of $\vec{r}_l$. The indices e, e^*, d correspond to processes

$$pN \to pN\,, \tag{12}$$

$$XN \to XN\,, \tag{12a}$$

and

$$pN \to XN . \tag{12b}$$

As intermediate states we have included in formula (11) only p and X.[12] We neglected longitudinal momentum transfer which is very small at our energies and missing-mass range,

$$q_l \simeq (M_X^2 - m_p^2)/2p_{\text{beam}} \leq 0.02 \text{ (GeV/}c\text{)} . \tag{13}$$

For the helium density we have used the uncorrelated wave function with the Gaussian one-particle distribution

$$\left|\psi(\vec{r}_1, \vec{r}_2, \vec{r}_3, \vec{r}_4)\right|^2 = \prod_{i=1}^{4} \left(\frac{1}{\sqrt{\pi}R}\right)^3 e^{-r_i^2/R^2} , \tag{14}$$

where $R = 1.36$ fm.

The proton-nucleon elastic amplitude was parametrized as follows:

$$f^e(\vec{q}) = \frac{ip\sigma}{4\pi}(1 - i\rho) \exp\left(-\frac{B}{2} q^2\right) , \tag{15}$$

where σ is the proton-nucleon total cross section, ρ is the ratio of the real to imaginary part, and B is the slope of the differential cross section.

In a similar way we parametrized the amplitude for $X - N$ elastic scattering,

$$f^{e*}(\vec{q}) = \frac{ip\sigma^*}{4\pi}(1 - i\rho^*) \exp\left(-\frac{B^*}{2} q^2\right) . \tag{15a}$$

For elementary diffraction dissociation we have considered two cases: central and peripheral diffraction-dissociation amplitudes.[2,13,14]

For the central case we used a spinless, purely imaginary amplitude with slopes determined from the fits to the cross sections for nucleon diffraction dissociation on protons,

$$f^d(\vec{q}) = \frac{ipg}{4\pi}\left[C \exp\left(-\frac{a_1}{2} q^2\right) + (1 - C) \exp\left(-\frac{a_2}{2} q^2\right)\right] , \tag{16}$$

where g, C, a_1, and a_2 are fitted parameters. The amplitude f^d is normalized in such a way that

$$\left.\frac{d^2\sigma}{dt\, dM_X^2}\right|_{pp \to Xp} = \frac{\pi}{p^2} \left|f^d(\vec{q})\right|^2 . \tag{17}$$

The profile function corresponding to amplitude (16) has a maximum at impact parameter $b = 0$, similarly to elastic scattering. With formulas (11), and (14)–(16) we obtained

$$\left.\frac{d^2\sigma}{dt\, dM_X^2}\right|_{p\,^4\text{He} \to X\,^4\text{He}} = \frac{\pi}{p^2} \left|F(\vec{q})\right|^2 , \tag{18}$$

where

$$F(\vec{q}) = ip \exp\left(\frac{R^2 q^2}{16}\right) \sum_{l=1}^{2} \sum_{n=1}^{4} \sum_{m=1}^{n} \binom{4}{n} (-1)^{n-1} A_l C_1^{n-m} C_2^{m-1} \frac{B_{l,n,m}}{2} \exp\left(-\frac{B_{l,n,m} q^2}{4}\right) , \tag{19}$$

TABLE III. Differential cross sections $d^2\sigma/dt\, dM_X^2$ in $\mu b(\text{GeV}/c)^{-2}\text{GeV}^{-2}$ for $p\,^4\text{He} \to X\,^4\text{He}$.

$-t$ [(GeV/c)^2] \ M_X^2 (GeV^2)	$p_{\text{beam}} = 46$ GeV/c $1.2 < M_X^2 < 1.4$	$1.4 < M_X^2 < 1.6$	$1.6 < M_X^2 < 1.8$	$1.8 < M_X^2 < 2.0$	$2.0 < M_X^2 < 2.2$	$2.2 < M_X^2 < 2.4$
0.04	2663 ± 362	5790 ± 314	6972 ± 424	10 683 ± 704		
0.05	2170 ± 103	3734 ± 99	4833 ± 141	6 643 ± 236	8707 ± 780	
0.06	1066 ± 68	2009 ± 74	3116 ± 111	4 342 ± 197	4091 ± 337	
0.07	730 ± 49	1346 ± 50	1705 ± 65	2 456 ± 120	3202 ± 160	
0.08	505 ± 31	915 ± 33	1120 ± 45	1 552 ± 80	2101 ± 103	
0.09	337 ± 24	707 ± 31	737 ± 36	822 ± 56	1278 ± 78	
0.10	278 ± 20	500 ± 26	612 ± 35	631 ± 51	1060 ± 70	
0.11	243 ± 19	292 ± 22	455 ± 32	509 ± 48	610 ± 58	
0.12	184 ± 18	301 ± 22	370 ± 31	316 ± 42	519 ± 55	
0.13	157 ± 17	320 ± 24	332 ± 27	345 ± 42	380 ± 42	434 ± 94
0.14	176 ± 17	209 ± 14	308 ± 19	299 ± 23	301 ± 25	416 ± 40
0.15	162 ± 14	187 ± 11	250 ± 16	272 ± 21	278 ± 22	242 ± 28
0.17	166 ± 9	184 ± 6	236 ± 9	264 ± 11	241 ± 12	225 ± 17
0.20	129 ± 9	148 ± 7	180 ± 9	232 ± 11	246 ± 15	151 ± 22
0.23	83 ± 16	101 ± 7	136 ± 8	190 ± 11	212 ± 18	
0.26		73 ± 6	92 ± 7	129 ± 12	144 ± 28	
0.29		46 ± 6	58 ± 8	85 ± 16		
0.32		32 ± 6	44 ± 11			
0.35		30 ± 15				

TABLE III. (*Continued.*)

p_{beam} = 97 GeV/c

$-t$ [(GeV/c)^2] \ M_X^2 (GeV^2)	$1.4<M_X^2<1.6$	$1.6<M_X^2<1.8$	$1.8<M_X^2<2.0$	$2.0<M_X^2<2.2$	$2.2<M_X^2<2.4$	$2.4<M_X^2<2.6$
0.04	4448 ± 418	6120 ± 321	9037 ± 393	9978 ± 294	8115 ± 360	6940 ± 354
0.05	2980 ± 157	3972 ± 206	6182 ± 210	7226 ± 157	6654 ± 213	5197 ± 184
0.06	1873 ± 157	2683 ± 130	3883 ± 201	4708 ± 130	4547 ± 175	3286 ± 145
0.07	1002 ± 80	1355 ± 83	2013 ± 90	2934 ± 88	2819 ± 87	2243 ± 85
0.08	715 ± 76	803 ± 57	1254 ± 61	1846 ± 70	1759 ± 64	1744 ± 77
0.09	516 ± 73	570 ± 46	757 ± 52	1129 ± 46	1358 ± 63	1339 ± 62
0.10	310 ± 70	349 ± 34	492 ± 33	805 ± 40	969 ± 43	825 ± 58
0.11		250 ± 31	373 ± 28	364 ± 30	621 ± 44	565 ± 56
0.12		267 ± 27	292 ± 25	364 ± 27	452 ± 36	384 ± 57
0.13		194 ± 29	292 ± 29	302 ± 34	390 ± 51	401 ± 57
0.14		209 ± 48	239 ± 26	272 ± 33	305 ± 44	236 ± 38
0.15		267 ± 34	262 ± 23	180 ± 21	262 ± 27	175 ± 22
0.17		248 ± 30	240 ± 12	211 ± 11	163 ± 12	140 ± 13
0.20			204 ± 14	179 ± 14	150 ± 15	121 ± 13
0.23			157 ± 24	115 ± 11	125 ± 16	
0.26			151 ± 34	86 ± 26		

p_{beam} = 97 GeV/c

$-t$ [(GeV/c)^2] \ M_X^2 (GeV^2)	$2.6<M_X^2<2.8$	$2.8<M_X^2<3.2$
0.07	2296 ± 129	2565 ± 192
0.08	1893 ± 99	2033 ± 144
0.09	1397 ± 117	1615 ± 125
0.10	1045 ± 88	1283 ± 97
0.11	794 ± 84	956 ± 92
0.12	570 ± 49	697 ± 155
0.13	309 ± 50	
0.14	308 ± 44	
0.15	292 ± 44	257 ± 41
0.17	176 ± 16	160 ± 22
0.20	163 ± 31	

p_{beam} = 230 GeV/c

$-t$ [(GeV/c)^2] \ M_X^2 (GeV^2)	$2.2<M_X^2<2.4$	$2.4<M_X^2<2.6$	$2.6<M_X^2<2.8$	$2.8<M_X^2<3.2$	$3.2<M_X^2<3.6$	$3.6<M_X^2<4.0$
0.04	7156 ± 294	5402 ± 251	6276 ± 328	5555 ± 269	3513 ± 97	2660 ± 97
0.05	3978 ± 182	4524 ± 92	4657 ± 138	4222 ± 105	2467 ± 46	2016 ± 46
0.06	3494 ± 142	3093 ± 84	3546 ± 153	3001 ± 80	1887 ± 43	1460 ± 38
0.07	1781 ± 147	1946 ± 55	2313 ± 86	1911 ± 53	1442 ± 32	1083 ± 23
0.08	1441 ± 70	1475 ± 73	1684 ± 59	1390 ± 32	1013 ± 27	854 ± 19
0.09	1054 ± 75	1027 ± 60	1206 ± 48	1059 ± 29	721 ± 18	629 ± 17
0.10	807 ± 62	698 ± 60	890 ± 46	750 ± 20	531 ± 15	457 ± 13
0.11	384 ± 116	493 ± 41	622 ± 40	534 ± 17	410 ± 13	341 ± 13
0.12	368 ± 73	429 ± 58	483 ± 43	380 ± 17	274 ± 12	258 ± 10
0.13		259 ± 27	274 ± 30	273 ± 12	169 ± 9	173 ± 8
0.14		200 ± 22	250 ± 19	228 ± 10	133 ± 5	121 ± 5
0.15			179 ± 10	132 ± 7	93 ± 4	94 ± 4
0.17			138 ± 8	91 ± 3	67 ± 2	58 ± 1
0.20				60 ± 3	40 ± 2	32 ± 1
0.23				40 ± 4	30 ± 3	22 ± 1
0.26				43 ± 7	23 ± 3	16 ± 1
0.29					19 ± 3	14 ± 3
0.32					11 ± 3	16 ± 3
0.35					11 ± 4	13 ± 3
0.38					7 ± 6	10 ± 4

TABLE III. (*Continued.*)

$-t$ [(GeV/c)^2] \ M_X^2 (GeV^2)	p_{beam} = 230 GeV/c		
	$4.0 < M_X^2 < 6.0$	$6.0 < M_X^2 < 8.0$	$8.0 < M_X^2 < 10.0$
0.04	1951 ± 74		
0.05	1632 ± 21	1057 ± 31	
0.06	1161 ± 17	743 ± 25	
0.07	860 ± 12	556 ± 14	434 ± 51
0.08	631 ± 8	417 ± 10	344 ± 24
0.09	454 ± 7	299 ± 8	231 ± 16
0.10	365 ± 7	238 ± 7	213 ± 15
0.11	252 ± 5	168 ± 7	138 ± 12
0.12	180 ± 5	141 ± 7	95 ± 11
0.13	139 ± 4	84 ± 5	70 ± 11
0.14	103 ± 2	76 ± 3	58 ± 3
0.15	78 ± 2	55 ± 2	42 ± 3
0.17	49 ± 1	35 ± 1	29 ± 1
0.20	30 ± 1	21 ± 1	18 ± 1
0.23	22 ± 1	13 ± 1	16 ± 2
0.26	16 ± 1	12 ± 1	12 ± 2
0.29	15 ± 1	10 ± 1	
0.32	12 ± 1	6 ± 1	
0.35	9 ± 1	8 ± 2	
0.38	8 ± 1		

$-t$ [(GeV/c)^2] \ M_X^2 (GeV^2)	p_{beam} = 347 GeV/c					
	$2.8 < M_X^2 < 3.2$	$3.2 < M_X^2 < 3.6$	$3.6 < M_X^2 < 4.0$	$4.0 < M_X^2 < 6.0$	$6.0 < M_X^2 < 8.0$	$8.0 < M_X^2 < 10.0$
0.04	4726 ± 147	3246 ± 122	2434 ± 134	1789 ± 29	1219 ± 32	739 ± 106
0.05	3967 ± 76	2528 ± 58	1874 ± 48	1420 ± 15	1019 ± 13	718 ± 22
0.06	2649 ± 66	1889 ± 62	1450 ± 43	1038 ± 13	765 ± 12	540 ± 15
0.07	2064 ± 56	1290 ± 31	980 ± 32	737 ± 8	526 ± 8	385 ± 9
0.08	1320 ± 44	961 ± 29	756 ± 23	562 ± 7	385 ± 6	301 ± 7
0.09	997 ± 47	674 ± 24	540 ± 18	438 ± 6	296 ± 5	220 ± 6
0.10	732 ± 51	526 ± 23	395 ± 15	323 ± 4	212 ± 4	172 ± 5
0.11	300 ± 73	312 ± 19	298 ± 13	230 ± 4	158 ± 4	125 ± 5
0.12		310 ± 28	212 ± 10	178 ± 3	118 ± 3	96 ± 5
0.13		148 ± 15	145 ± 12	127 ± 3	83 ± 3	72 ± 4
0.14		128 ± 13	106 ± 7	95 ± 2	60 ± 2	50 ± 2
0.15		130 ± 24	86 ± 5	70 ± 2	54 ± 1	37 ± 1
0.17		81 ± 10	51 ± 2	45 ± 1	30 ± 1	27 ± 1
0.20			32 ± 3	28 ± 1	20 ± 1	15 ± 1
0.23				20 ± 1	14 ± 1	11 ± 1
0.26				14 ± 1	10 ± 1	9 ± 1
0.29				11 ± 1	9 ± 1	7 ± 1
0.32				8 ± 1	7 ± 1	5 ± 1
0.35				8 ± 1	5 ± 1	4 ± 1
0.38				5 ± 1	4 ± 1	

where

$$A_1 = \frac{gC}{2\pi(R^2 + 2a_1)} , \tag{20}$$

$$A_2 = \frac{g(1-C)}{2\pi(R^2 + 2a_2)} , \tag{20'}$$

$$C_1 = \frac{\sigma(1-\rho)}{2\pi(R^2 + 2B)} , \tag{21}$$

$$C_2 = \frac{\sigma^*(1-\rho^*)}{2\pi(R^2 + 2B^*)} , \tag{21'}$$

$$\frac{1}{B_{l,n,m}} = \frac{1}{R^2 + 2a_l} + (n-m)\frac{1}{R^2 + 2B} + (m-1)\frac{1}{R^2 + 2B^*} . \tag{22}$$

For the central case the coherent diffraction-dis-

sociation cross section shows similar behavior to elastic proton-helium scattering, i.e., it has a dip as a result of destructive interference between terms corresponding to the single and multiple interactions.

For the peripheral case elementary diffraction dissociation is described by a set of several helicity-flip amplitudes, each of them parametrized as follows[2]:

$$f^d_{\Delta\lambda}(\vec{q}) = \frac{ip}{4\pi} g_{\Delta\lambda} \exp\left(-\frac{a}{2} q^2\right) J_{\Delta\lambda}(b_0 q) \exp(i\Delta\lambda\phi) , \tag{23}$$

where $\Delta\lambda$ is an amount of helicity flip in the production vertex, $J_{\Delta\lambda}$ is the Bessel function of order $\Delta\lambda$, and ϕ is the azimuthal angle of $\vec{q}$. It is assumed, as in Ref. 13, that the spin state of the target nucleon is unchanged. The differential cross section for elementary diffraction dissociation is then

$$\left.\frac{d^2\sigma}{dt\,dM_X^2}\right|_{pp\to Xp} = \frac{\pi}{p^2} \sum_{\Delta\lambda=0}^{\Delta\lambda_{max}} |f^d_{\Delta\lambda}(\vec{q})|^2 \tag{24}$$

and usually[2,13] $\Delta\lambda_{max} \leq 4$. The profile functions corresponding to (23) are peaked at impact parameter $b \simeq b_0$. For the peripheral case we calculated each helicity-flip amplitude for process (1) separately and, using (11), (14), (15), and (23), we got

$$F_{\Delta\lambda}(\vec{q}) = ip \exp\left(\frac{R^2 q^2}{16}\right) \sum_{n=1}^{4} \sum_{m=1}^{n} \binom{4}{n} (-1)^{n-1} A_{\Delta\lambda} C_1^{\,n-m} C_2^{\,m-1} \frac{B_{n,m}}{2}$$

$$\times J_{\Delta\lambda}\left(b_0 q \frac{B_{n,m}}{B_{1,1}}\right) \exp\left(-\frac{B_{n,m} q^2}{4}\right) \exp\left(-b_0^2 \frac{B_{1,1} - B_{n,m}}{B_{1,1}^2}\right) , \tag{25}$$

where

$$A_{\Delta\lambda} = \frac{g_{\Delta\lambda}}{2\pi(R^2 + 2a)} . \tag{26}$$

C_1 and C_2 are defined by (21) and $B_{n,m}$ by a formula analogous to (22) except now there is no index l. The differential cross section for reaction (1) is

$$\left.\frac{d^2\sigma}{dt\,dM_X^2}\right|_{p\,^4\mathrm{He}\to X\,^4\mathrm{He}} = \frac{\pi}{p^2} \sum_{\Delta\lambda} |F_{\Delta\lambda}|^2 . \tag{27}$$

Helicity-flip amplitudes given by (25) were obtained in the approximation of near-forward production and elastic scattering. The approximation is well justified for this experiment.

It is worth stressing that as in the Humble model of peripheral diffraction dissociation,[13] the helicity flips take place only in the production vertex; so within the framework of this model it is not expected that there will be any suppression of the cross section for production on helium due to spin effects.

Peculiar features of coherent peripheral diffraction dissociation on nuclei, as discussed in detail in Ref. 2 for the deuteron, include the existence of interference terms of both types, destructive and constructive, depending on t range and an appearance of diffractive minima and maxima at different t values for different helicity-flip amplitudes.

B. Analysis of experimental data

We compared our experimental momentum-transfer distributions with the predictions of Glauber formulas (18)–(22) and (25)–(27).

The proton-nucleon elastic amplitude was parametrized with (15) using the same values for σ, ρ, B as for proton-proton elastic scattering.[15] For the elastic scattering of a diffractively produced state X on a nucleon, we assumed $B^* = B$, $\rho^* = 0$ and we considered two variants: one with $\sigma^* = 20$ mb and another with $\sigma^* = 40$ mb.[2,16,17]

Existing high-resolution data on the inclusive process $pp \to Xp$ unfortunately do not cover all the mass range of our experiment. At small masses, below and near the two-pion production threshold, we have used Fermilab data[18] on the exclusive reaction $np \to (p\pi^-)p$ and for high masses, $M_X^2 \geq 4$ GeV^2, we have used data on the inclusive reaction (2) from the Single Arm Spectrometer group.[3] Unfortunately, we lack good input for our analysis for intermediate masses. Although there exist precise data on inclusive proton dissociation on protons[4] in this mass range, they are not particularly useful for our analysis because the t range they cover is too narrow.

The amplitudes of elementary proton diffraction dissociation which we used in the Glauber analysis were parametrized as (16), (17) for the central case, and as (23), (24) for the peripheral case with the parameters found in the fits to the data of Refs. 3 and 18. Before applying the small-mass data on the exclusive reaction $np \to p\pi^- p$ to our analysis we renormalized them by an isospin factor $\frac{3}{2}$.

For the peripheral case we have used explicitly an assumption of the Humble model,[13] i.e., that parameters a and b_0 of (23) are the same for all

masses. We have included the minimum number of helicity-flip amplitudes necessary to reproduce the data with good χ^2. For small masses it was sufficient to include $\Delta\lambda = 0, 1$, and for high masses $\Delta\lambda = 0, 1, 2, 3$.

The Glauber-model predictions for central and peripheral amplitudes are compared with our data in Fig. 7. For central diffraction dissociation the model predicts the t dependence similar to that of elastic proton-helium scattering, i.e., the presence of a dip at $|t| \simeq 0.10$–0.18 $(\mathrm{GeV}/c)^2$ arising from destructive interference between terms corresponding to single and multiple interactions. For peripheral diffraction dissociation there is no dip and cross sections are larger. This is mainly due to the incoherent contribution of terms (25) corresponding to different helicity flips, each having interference minima and maxima at different t values. Also to some extent the cross sections for t in the range $|t| > 0.17$ $(\mathrm{GeV}/c)^2$ are enhanced due to constructive interference between single- and double-scattering terms for the non-helicity-flip amplitude $\Delta\lambda = 0$.

The t dependence of the experimental data is substantially different from the model predictions for central diffraction dissociation. In the case of peripheral diffraction dissociation the shape of the predicted curves is in much better agreement with the data. As for absolute values of cross sections, for peripheral diffraction dissociation the predicted values are on an average about 30% lower than the experimental data for small masses and about 70% higher than the data for large masses. In view of systematic errors in the helium and proton data and approximations of the model, the difference at small masses is not significant. However, for large masses it cannot be explained completely by the same effects. A possible explanation of the difference at large masses may be a contribution of amplitudes with helicity flip of the target nucleon in reaction (2). For coherent diffraction dissociation on helium such amplitudes would be suppressed.

To illustrate how diffraction dissociation on helium is sensitive to the absorption of the pro-

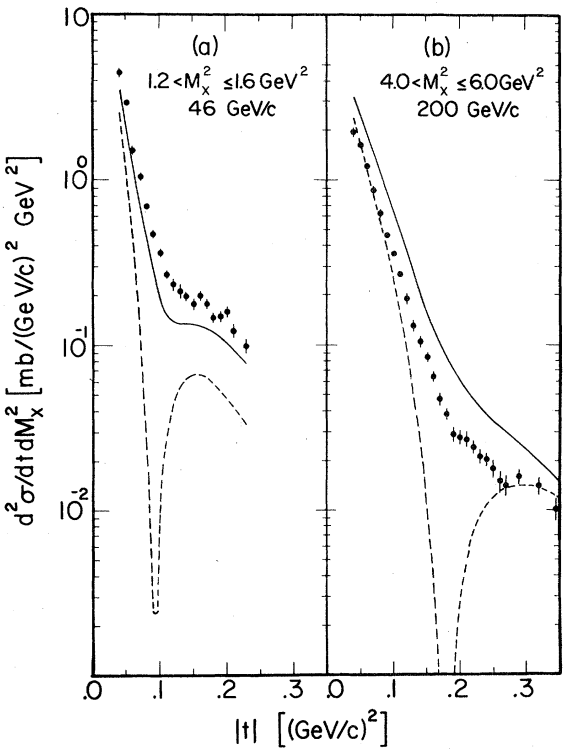

FIG. 7. Differential cross sections for $p\,^4\mathrm{He} \to X\,^4\mathrm{He}$ as functions of t. Solid lines represent the Glauber-model predictions with peripheral elementary proton diffraction dissociation, dashed ones with central diffraction dissociation. (a) Mass range $1.2 < M_X^2 < 1.6$ GeV^2, total cross section $\sigma^*(XN) = 40$ mb. (b) Mass range $4 < M_X^2 < 6$ GeV^2, $\sigma^*(XN) = 40$ mb.

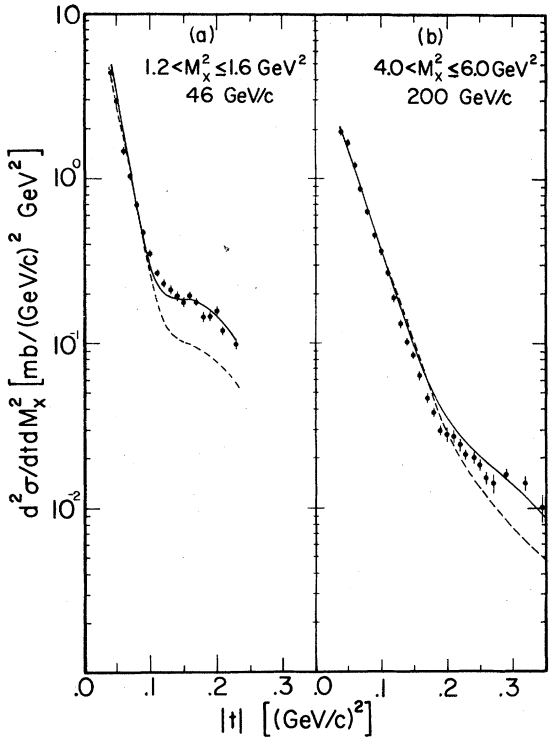

FIG. 8. Differential cross sections for $p\,^4\mathrm{He} \to X\,^4\mathrm{He}$. Curves are Glauber-model predictions with peripheral elementary diffraction dissociation normalized to experimental data at small-$|t|$ values [$|t| \leq 0.1$ Gev/$c)^2$]. The solid lines are obtained for total cross section $\sigma^*(XN) = 40$ mb and the dashed ones with $\sigma^*(XN) = 20$ mb. (a) Mass range $1.2 < M_X^2 < 1.6$ GeV^2. (b) Mass range $4 < M_X^2 < 6$ GeV^2.

duced state in subsequent collisions we plot in Fig. 8 Glauber-model predictions for the peripheral case with $\sigma^* = 20$ mb and $\sigma^* = 40$ mb, together with experimental data. The theoretical curves are normalized to the data at small $|t|$ values $[|t| \leq 0.1\ (\mathrm{GeV}/c)^2]$. At small masses the agreement is much better for $\sigma^* = 40$ mb. The comparison is not so conclusive for large masses and probably a more refined model would be helpful to solve the ambiguity.

V. CONCLUSIONS

Inclusive coherent proton diffraction dissociation on helium has been measured using the circulating beam in the Fermilab accelerator intercepting a thin helium gas-jet target. The recoil helium nuclei were detected with sandwiches of solid-state detectors. The t, missing-mass, and momentum ranges were $0.04 < |t| < 0.40\ (\mathrm{GeV}/c)^2$, $(m_p + m_\pi)^2 < M_X{}^2 < 10\ \mathrm{GeV}^2$, and $46 < p_{\mathrm{beam}} < 400\ \mathrm{GeV}/c$.

The characteristic features of the mass distributions are a large enhancement at $M_X{}^2 \simeq 2\ \mathrm{GeV}^2$ and a high-mass tail decreasing approximately as $1/M_X{}^2$. At small $|t|$ values the relative contribution of the 2-GeV^2 enhancement decreases with increasing $|t|$, but starting from $|t|$ of about 0.14 $(\mathrm{GeV}/c)^2$ it becomes large again.

At small momentum transfers the differential cross sections are sharply decreasing functions of $|t|$ with the slope-parameter values reflecting the helium form factor and the slope of elementary proton diffraction dissociation. The slope-mass correlation for small-momentum-transfer data for helium and proton targets are similar. At large momentum transfers the t dependence of helium differential cross sections is governed by multiple-scattering processes yielding small values of slope.

Within the framework of a simplified Glauber model we find the cross section of the coherent diffraction dissociation on helium is very sensitive to the details of the amplitude of elementary proton diffraction dissociation and on the total cross sections of the diffractively produced states on nucleons, $\sigma^*(XN)$. We find that by using central elementary diffraction dissociation one arrives at predictions which are substantially different from the data, whereas for peripheral diffraction dissociation it is possible to reproduce the shape of the cross sections.

The disagreement in absolute values of cross sections between the high-mass data and a simplified Glauber model may be only partly of an experimental origin. A possible explanation of it could be a contribution of amplitudes with spin flip of the target nucleon in reaction (2).

ACKNOWLEDGMENTS

We acknowledge the strong support of the Fermilab Internal Target Group led by Dr. T. Nash and the Fermilab Accelerator Division led by Dr. Russ Huson. We are grateful to Professor Valdimir Kadeshevsky for his help. The Dubna members of the collaboration wish to acknowledge the hospitality of the Fermilab Directorate during their stay. This work was supported in part by the U. S. Department of Energy, the U. S. National Science Foundation, and the U. S. S. R. State Committee For Atomic Energy.

---

*Present address: Purdue University, Lafayette, Indiana 47907.
†Permanent Address: Institute of Technology and Chemistry, Sofia, Bulgaria.
‡Permanent Address: KEK, Ibaraki-Ken, Japan.

[1]A. Bujak *et al.*, preceding paper, Phys. Rev. D 23, 1895 (1981).
[2]G. Goggi *et al.*, Lett. Nuovo Cimento 24, 381 (1979); Nucl. Phys. B161, 14 (1979); G. Alberi and G. Goggi, Lett. Nuovo Cimento 27, 229 (1980).
[3]D. S. Ayres *et al.*, Phys. Rev. Lett. 37, 1724 (1976); R. L. Anderson *et al.*, *ibid.* 38, 880 (1977).
[4]A. A. Kuznetsov *et al.*, Yad. Fiz. 30, 1018 (1979) [Sov. J. Nucl. Phys. 30, 529 (1979)].
[5]V. Bartenev *et al.*, Phys. Lett. 51B, 299 (1974).
[6]S. Childress *et al.*, Phys. Lett. 65B, 177 (1976).
[7]Y. Akimov *et al.*, Phys. Rev. Lett. 39, 1432 (1977).
[8]Y. Akimov *et al.*, Phys. Rev. Lett. 35, 763 (1975); 35, 766 (1975).
[9]R. J. Glauber, in *Lectures in Theoretical Physics*, edited by W. E. Brittin and L. G. Dunham (Interscience, New York, 1959), Vol. 1, p. 315.
[10]W. Czyż and L. Leśniak, Phys. Lett. 24B, 227 (1967).
[11]Miyo Ikeda, Phys. Rev. C 6, 1608 (1972).
[12]K. Kölbig and B. Margolis, Nucl. Phys. B6, 85 (1968).
[13]S. Humble, Nucl. Phys. B76, 137 (1974); B86, 285 (1975).
[14]G. Fäldt and P. Osland, Nucl. Phys. B126, 221 (1977).
[15]D. Gross *et al.*, Phys. Rev. Lett. 41, 217 (1978).
[16]W. Mollet *et al.*, Phys. Rev. Lett. 39, 1646 (1977).
[17]R. M. Edelstein *et al.*, Phys. Rev. Lett. 38, 185 (1977).
[18]J. Biel *et al.*, Phys. Rev. D 18, 3079 (1978).